Journal of Hazardous Materials 173 (2010) 102–109

Contents lists available at ScienceDirect

Journal of Hazardous Materials

journal homepage: www.elsevier.com/locate/jhazmat

Removal of fluoride from aqueous media by Fe_3O_4@Al(OH)$_3$ magnetic nanoparticles

Xiaoli Zhao[a,b], Jieming Wang[a], Fengchang Wu[b], Thanh Wang[a], Yaqi Cai[a,*], Yali Shi[a], Guibin Jiang[a]

[a] State Key Laboratory of Environmental Chemistry and Ecotoxicology, Research Center for Eco-Environmental Sciences, Chinese Academy of Sciences, Beijing 100085, China
[b] State Environmental Protection Key Laboratory for Lake Pollution Control, Chinese Research Academy of Environmental Sciences, Beijing 100012, China

ARTICLE INFO

Article history:
Received 16 January 2009
Received in revised form 12 June 2009
Accepted 12 August 2009
Available online 20 August 2009

Keywords:
Fluoride
Magnetic nanosized adsorbent
Hydrous aluminum oxide

ABSTRACT

A novel magnetic nanosized adsorbent using hydrous aluminum oxide embedded with Fe_3O_4 nanoparticle (Fe_3O_4@Al(OH)$_3$ NPs), was prepared and applied to remove excessive fluoride from aqueous solution. This adsorbent combines the advantages of magnetic nanoparticle and hydrous aluminum oxide floc with magnetic separability and high affinity toward fluoride, which provides distinctive merits including easy preparation, high adsorption capacity, easy isolation from sample solutions by the application of an external magnetic field. The adsorption capacity calculated by Langmuir equation was 88.48 mg g^{-1} at pH 6.5. Main factors affecting the removal of fluoride, such as solution pH, temperature, adsorption time, initial fluoride concentration and co-existing anions were investigated. The adsorption capacity increased with temperature and the kinetics followed a pseudo-second-order rate equation. The enthalpy change (ΔH^0) and entropy change (ΔS^0) was 6.836 kJ mol^{-1} and 41.65 J mol^{-1} K^{-1}, which substantiates the endothermic and spontaneous nature of the fluoride adsorption process. Furthermore, the residual concentration of fluoride using Fe_3O_4@Al(OH)$_3$ NPs as adsorbent could reach 0.3 mg L^{-1} with an initial concentration of 20 mg L^{-1}, which met the standard of World Health Organization (WHO) norms for drinking water quality. All of the results suggested that the Fe_3O_4@Al(OH)$_3$ NPs with strong and specific affinity to fluoride could be excellent adsorbents for fluoride contaminated water treatment.

1. Introduction

Fluoride contamination in the drinking water due to natural reasons and human activities is a major problem worldwide [1,2]. According to World Health Organization (WHO) norms, the upper limit of fluoride concentration in drinking water is 1.5 mg L^{-1} [3]. Long-term ingestion of high-fluoride drinking water can cause fluorosis [4,5], which is a chronic disease manifested by mottling of teeth in mild cases, softening of bones ossification of tendons and ligaments and neurological damage in severe cases [2,6]. Millions of people in the world are affected by fluorosis, especially in Asian countries such as China, India, Pakistan, and Thailand [6–8].

Several methods have been applied to remove excessive fluoride from aqueous environments, such as adsorption [2,8–10], precipitation [6], ion-exchange [11], electrodialysis [12] and electrochemical methods [13]. Among them, precipitation and adsorption are two most important techniques used for water defluoridation. Precipitation methods based on the addition of chemicals to the water is simple and economical, and is used principally for the treatment of high-fluoride containing wastewater (typically greater than 10 mg L^{-1}). But, the final concentration of fluoride is generally still above level prescribed by WHO and excess chemicals in treated water are difficult to eliminate. For example, the theoretical lower concentration limit of fluoride in treated water using limestone (CaO) as precipitation reagent is approximately 2 mg L^{-1} [6]. Comparatively, adsorption seems to be the most attractive method for the removal of fluoride below 1 mg L^{-1}. The criteria for the selection of adsorbent mainly include its potential (adsorption capacity) for fluoride removal and the cost. Various low-cost materials such as activated alumina [7,8], clay [14], soil [15], bone char [8,12], light weight concrete [16], fly ash and other materials [2,13] have been tested for removing fluoride from drinking water, but the fluoride adsorption capacities of those materials are not high enough for wide application [8]. In the past few years, novel adsorbents with strong affinity towards fluoride have been developed for fluoride removal, such as synthetic ion exchangers calcined Mg–Al–CO_3 layered double hydroxides (LDH) [7], zirconium-impregnated collagen fiber [2], Fe–Al–Ce trimetal oxide [17] and iron-aluminum mixed oxide [9]. Rare earth elements also have been investigated as potential adsorbents because of their selective affinity to fluoride, high adsorption capacity, cause little pollution, and easy preparation [18]. These

* Corresponding author at: Research Center for Eco-Environmental Sciences, Chinese Academy of Sciences, P.O. Box 2871, Beijing 100085, China.
Tel.: +86 010 62849239; fax: +86 010 62849182.
E-mail address: caiyaqi@rcees.ac.cn (Y. Cai).

0304-3894/$ – see front matter © 2009 Elsevier B.V. All rights reserved.
doi:10.1016/j.jhazmat.2009.08.054

novel adsorbents have shown very promising fluoride adsorption capacities, but some of them are expensive to be considered for full scale drinking water treatment. Furthermore, the adsorption processes of those adsorbents generally involve the passage of raw water through an adsorbent bed and the initial setup cost is high. Therefore, an effective and low-cost adsorbent with high-fluoride adsorption capacity and efficient treatment technology for removal of fluoride from large volume water samples is desirable.

Most of adsorbents for removing fluoride reported in literatures are micron-sized particles. In recent years, nanomaterials have attracted much interest and been widely used as sorbents due to properties such as high surface-to-volume ratio and short diffusion route [19]. Because of comparatively large surface areas, it is likely that nanosized adsorbents with strong affinity towards fluoride can be a useful tool in enhancing the adsorption capacity in drinking water treatment. However, due to their small particle size, isolation of nanosized adsorbents from matrices is difficult for practical application. Magnetic nanosized adsorbents overcome the shortcoming of nonmagnetic nanomaterials and are very promising for application in the field of preconcentration and removal pollutants from environmental samples [19–23].

Hydrous aluminum oxide $Al(OH)_3$ floc, a well-known high affinity adsorbent toward fluoride, has recently been used as cost-efficient adsorbents for large-scale defluoridation with good results [10,24]. Fluoride is adsorbed on oppositely charged hydrous aluminum oxide surface by strong electrostatic force and a probable chemical reaction that occurs on the surface is:

$$[Al(OH)_3] + xF^- \rightarrow Al(OH)_{3-x}F_x + xOH^- \quad (1)$$

If one combines the advantages of $Al(OH)_3$ and magnetic nanoparticles to fabricate nanosized adsorbents with high surface area, high affinity toward fluoride and good magnetic separability, a new kind of magnetic fluoride adsorbent may be obtained.

In the present work, we successfully synthesized Fe_3O_4@$Al(OH)_3$ NPs and investigated the adsorption feasibility of this nanomaterial for fluoride. A simple defluoridation method, based on magnetic carrier technology (MCT) [25–28] and nanosized adsorbent, was established. The Fe_3O_4@$Al(OH)_3$ NPs could offer several advantages over traditional micron-sized adsorbents; they possess not only high surface area which leads to higher adsorption capacity, but also strong superparamagnetic properties which can meet the need of rapid treatment of large volume water samples by employing a strong external magnetic field.

2. Experimental

2.1. Chemicals and materials

All reagents were of analytical reagent-grade and were used as supplied. Aluminum nitrate nonahydrate ($Al(NO_3)_3{\cdot}9H_2O$), ferric chloride ($FeCl_3{\cdot}6H_2O$), ferrous chloride ($FeCl_2{\cdot}4H_2O$) and sodium fluoride (NaF, analytical reagent (AR) grade) were purchased from Beijing Chemicals Corporation (Beijing, China). Standard stock solutions of fluoride (1000 mg L^{-1} or 52 mmol/L F) were prepared by dissolving 0.221 g sodium fluoride into 100 mL deionized water and stored under dark conditions at 4 °C. Deionized water used in all of the experiments was prepared using Milli-Q water by Milli-Q system (Millipore, Bedford, MA).

2.2. Preparation of magnetic adsorbents

The Fe_3O_4 nanoparticles were prepared by chemical coprecipitation methods as reported in our previous works [19–21] and the Fe_3O_4@$Al(OH)_3$ NPs were synthesized according to previous reported methods with minor modification [10]. 5.2 g of $FeCl_3{\cdot}6H_2O$, 2.0 g of $FeCl_2{\cdot}4H_2O$ and 0.85 mL of HCl (12 mol/L) were dissolved in 25 mL of deionized water (degassed with nitrogen gas before use). Then, the solution was added dropwise into 250 mL of 1.5 M NaOH solution under vigorous stirring using nonmagnetic stirrer at 80 °C. The obtained Fe_3O_4 nanoparticles were separated from the reaction medium by magnetic field, and washed with 200 mL deionized water four times, then resuspended in 100 mL deionized water.

1 M aluminum nitrate was added dropwise into the Fe_3O_4 NPs suspension and the pH value of the mixture was adjusted to 8.0 by addition of 2 M NaOH within 1 h. The mixture was stirred for 2 h after the addition. During the whole process, temperature was maintained at 80 °C and nitrogen gas was used to prevent the intrusion of oxygen. The mass ratio of Fe_3O_4 to $Al(OH)_3$ was 2:3, 2:5, 2:6 by varying the proportion of $Al(OH)_3$ to Fe_3O_4 NPs suspension and the resulting particles was termed as Fe_3O_4@$Al(OH)_3$ (2:3), Fe_3O_4@$Al(OH)_3$ (2:5) and Fe_3O_4@$Al(OH)_3$ (2:6), respectively. Finally, the formed NPs were then thoroughly washed with deionized water and resuspended in deionized water. The concentration of the generated nanoparticles suspension was estimated to be about 20 mg mL^{-1} (Fe_3O_4@$Al(OH)_3$ (2:5)).

2.3. Sample collection

Ground water and surface water samples were obtained from different districts of Beijing. Surface water samples were collected from Jingmi Canal (Haidian District, Beijing) in July 2008. Tap water samples were taken from our lab in Haidian District, Beijing and a ground water samples were obtained from the campus of China Agricultural University.

2.4. Ion chromatography analysis and characterization

The determination of fluoride was performed utilizing an ICS-2500 ion chromatography (Dionex, U.S.A.). This instrument was equipped with a gradient pump module, a conductivity detector, and an anion exchange column specifically designed for the rapid analysis of inorganic anion (DIONEX IonPac AS22). An IonPac AG-22 column was placed in-line prior to the analytical column. For enhanced sensitivity, the eluent was pumped through an anion self resuppressor (DIONEX ASRS-I) before delivery to the conductivity detector. The anions were eluted isocratically at a flow rate of 1.0 mL min^{-1} using a carbonate/bicarbonate eluent. The eluent was prepared according to the manufacturer's recommendation (4.5 mM Na_2CO_3, 1.4 mM $NaHCO_3$). The injection volume was 50 μL and three replicate injections were made for each sample.

The specific surface areas of adsorbents were determined by the BET method with N_2 gas (ASAP2000V3.01A; Micromeritics, Norcross, GA). The particle size was determined with a laser particle size analyser (Malvern, UK). Morphology of the samples was determined by scanning electron microscope (SEM) with S-3000N (Hitachi, Japan). X-ray powder diffractometer (XRD, Rigaku III/B max) was used to analyze the composition crystalline structures of adsorbents. The radiation source was Cu Kα. The applied current was 30 mA and the voltage was 40 kV. X-ray photoelectron spectroscopy (XPS) measurements were conducted by using ESCA-Lab-220i-XL spectrometer with monochromatic Al Kα radiation (1486.6 eV). C 1s peaks were used as an internal standard calibration peak at 284.7 eV. XPS data processing and peak fitting was preformed using a nonlinear least-squares fitting program (XPS peak software 4.1, Raymund W.M. Kwork). Zeta potential measurements of Fe_3O_4@$Al(OH)_3$ NPs were performed with a Zetasizer 2000 apparatus (Malvern, United Kingdom). Magnetic properties were analyzed using a vibrating sample magnetometer (VSM, LDJ9600).

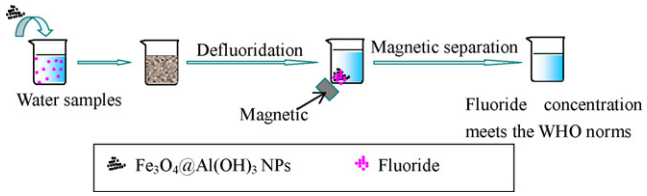

Scheme 1. Schematic illustration of the defluoridation procedure using Fe_3O_4@$Al(OH)_3$ NPs as adsorbents.

2.5. Isotherm studies

The defluoridation procedure using Fe_3O_4@$Al(OH)_3$ NPs as adsorbents allowed rapid separation by a simple magnetic extraction method. Illustration of the whole treatment procedure can be followed in Scheme 1. Equilibrium isotherm experiments were conducted with initial fluoride concentrations ranging in 0–160 mg L^{-1} using batch procedure at 25 ± 1 °C in deionized water. 2.5 mL of Fe_3O_4@$Al(OH)_3$ NPs (20 mg mL^{-1}) suspension was added into 50 mL of deionized water and placed in an inert 100 mL polyethylene bottle. The initial pH value of the water solution was adjusted to about 6.5 with 1 M NaOH or HCl. All of the equilibrium experiments were carried out at 25 ± 1 °C in water bath with vigorous stirring under 1 h. Then, an Nd–Fe–B strong magnet (rectangular shape, 150 mm × 130 mm × 50 mm, maximum energy product 52 MGOe) was deposited at the bottom of the bottle and the magnetic adsorbents were isolated from their suspension. After a few seconds, the suspension became limpid. 5 mL of supernatant liquid was passed through an On-guard H column (Dionex, U.S.A.) to remove cations and then analyzed for the remaining fluoride concentration with ion chromatography (ICS-2500, Dionex, U.S.A.). Effect of initial solution pH on the adsorption of analytes was investigated with fixed fluoride concentrations (20, 40 and 60 mg L^{-1}) and adsorbents amounts (1 mg mL^{-1}) at different initial pH (pH 5–9). Duplicate adsorption experiments were conducted, and averaged results were reported.

2.6. Kinetic studies

The time-dependent adsorption reactions were conducted by agitation at 280 rpm of the reaction mixture that was placed in water bath. Herein, 0.5 g of Fe_3O_4@$Al(OH)_3$ NPs were thoroughly mixed with 500 mL of a fluoride solution with fixed initial fluoride concentrations (20, 40 and 60 mg L^{-1}). At a fixed preselected time interval from 0.1 to 240 min, 2 mL reaction mixture was withdrawn by a micropipette and analyzed for residual fluoride. The above adsorption reaction was conducted separately at a definite temperature (25, 40 and 50 °C).

The effects of co-existing anions (phosphate, nitrate, chloride, bromide and sulfate) on fluoride adsorption were investigated by performing fluoride adsorption under a fixed adsorbent dose of 1 mg mL^{-1}, initial concentration of each co-existing anions of 50 mg L^{-1}, solution initial pH of 6.5 ± 0.1.

3. Results and discussion

3.1. Characterization of Fe_3O_4@$Al(OH)_3$ adsorbents

The specific surface area of Fe_3O_4@$Al(OH)_3$ NPs (2:5) were determined to be 147 m^2/g. The SEM image (Fig. 1) of Fe_3O_4@$Al(OH)_3$ NPs (2:5) clearly reveals the floc and porosity surface texture, which endows the adsorbents with large surface areas and high adsorption capacity. Several monodisperse Fe_3O_4 NPs with diameters of 10 nm embedded in $Al(OH)_3$ floc forming nano-sized or sub-micron-sized magnetic particles. As shown in Fig. 2, the

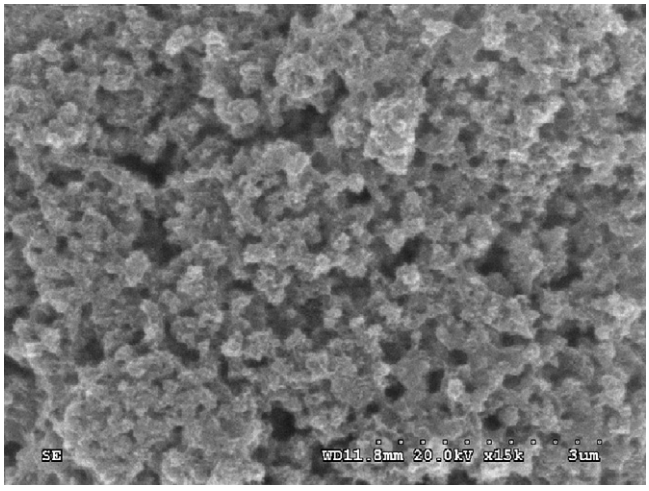

Fig. 1. SEM of Fe_3O_4@$Al(OH)_3$ (2:5) NPs.

particle size distribution curve of Fe_3O_4@$Al(OH)_3$ NPs (2:5) indicated that main particle size of this particle was in the range of 240–340 nm. The XRD patterns of pure Fe_3O_4 and Fe_3O_4@$Al(OH)_3$ (2:5) NPs (Fig. 3) clearly revealed the existence of hydrous aluminum in the resulting nanoparticles. As shown in curve b of Fig. 3, the diffraction peaks at 2θ = 18.7°, 20.2°, 27.8°, 40.5°, 53.1° and 57.3° can be respectively indexed to (0 0 1), (1 1 0, 0 2 0), (1 1 1, 0 2 1), (2 0 1, 1 3 1), (2 0 2, 1 3 2) and (2 2 0, 0 4 2) planes of hydrous aluminum in bayerite structure. Detailed information about the surface of resulting nanoparticles, the $Al(OH)_3$ layer coating on Fe_3O_4 nanoparticles, were further confirmed by XPS. Since XPS generally provides elemental information at depth of only a few atomic layers, it is routinely applied to characterizing surface composition [28]. As shown in Fig. 4, after the Fe_3O_4 NPs was coated with $Al(OH)_3$, the signals for Fe 2p disappeared while only Al peaks was observed (curve b of Fig. 4). It can be attributed to the fact that $Al(OH)_3$ deposited on the surface of the magnetic core to a greater degree and the $Al(OH)_3$ layer was thick enough to cover the substrate metals. Furthermore, compared with the standard spectrum of A1, the XPS spectrum of Fe_3O_4@$Al(OH)_3$ NPs (curve b of Fig. 4) showed characteristic peaks at binding energy of 118.1 and 74.2 eV which were assigned to the Al 2s and Al 2p and demonstrated the bayerite structure of $Al(OH)_3$ coating.

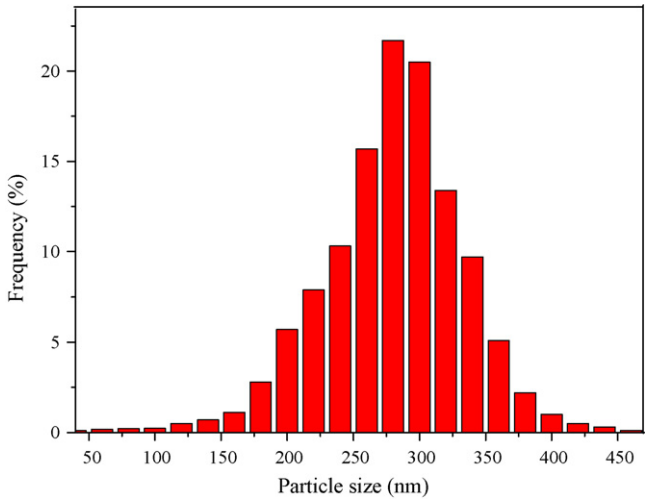

Fig. 2. Size distribution plot of Fe_3O_4@$Al(OH)_3$ (2:5) NPs.

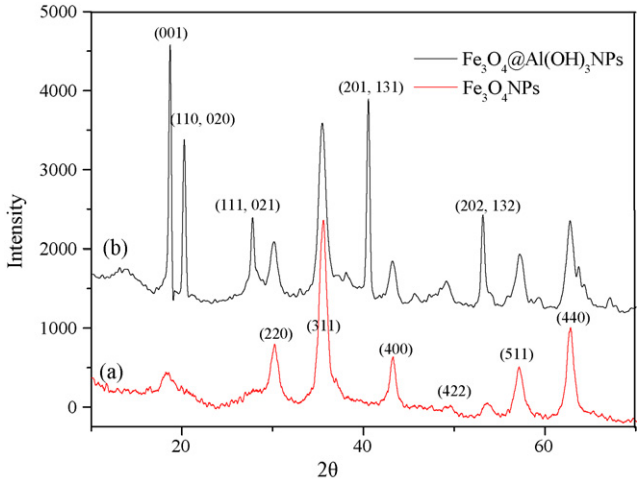

Fig. 3. X-ray powder diffractometer (XRD) for Fe_3O_4 NPs (a) and Fe_3O_4@$Al(OH)_3$ NPs (b).

3.2. Magnetic property of Fe_3O_4@$Al(OH)_3$ NPs

A distinct advantage of this defluoridation procedure is that the adsorbents can readily be isolated from sample solutions by the application of an external magnetic field. These adsorbents are superparamagnetic, therefore, suspended superparamagnetic adsorbents can adequately disperse into the solution; while after tagging with fluoride, they can be removed from the water samples by applying a magnetic field. Fig. 5 shows the VSM magnetization curves of Fe_3O_4 NPs, Fe_3O_4@$Al(OH)_3$ NPs at room temperature. All of the magnetic nanoparticles exhibited typical superparamagnetic behavior, characterized with strong magnetic susceptibility and no hysteresis, remanence and coercivity. Saturation magnetization, a measure of the maximum magnetic strength, is a key factor for successful magnetic separation. Due to the weight contribution from the nonmagnetic $Al(OH)_3$, the increase in the mass of $Al(OH)_3$ results in the decrease in the magnetic strength of the adsorbents. The saturation magnetization of Fe_3O_4, Fe_3O_4@$Al(OH)_3$ (2:3), Fe_3O_4@$Al(OH)_3$ (2:5) and Fe_3O_4@$Al(OH)_3$ (2:6) were 63.2, 24.6, 17.9 and 15.8 emu/g, respectively. Ma et al. [29] found that a saturation value of 16.3 emu/g was sufficient for magnetic separation with a conventional magnet. Thus, the saturation magnetization value achieved with Fe_3O_4@$Al(OH)_3$ (2:5) NPs was high enough for magnetic separation.

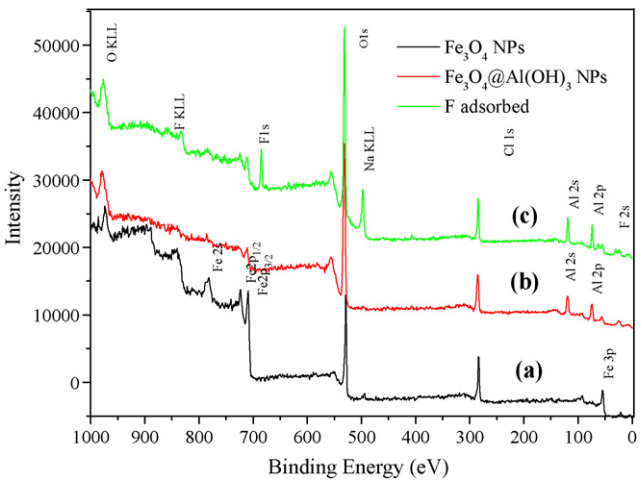

Fig. 4. The X-ray photoelectron spectroscopy (XPS) survey spectra of pure Fe_3O_4 NPs, Fe_3O_4@$Al(OH)_3$ NPs and Fe_3O_4@$Al(OH)_3$ NPs with fluoride adsorbed.

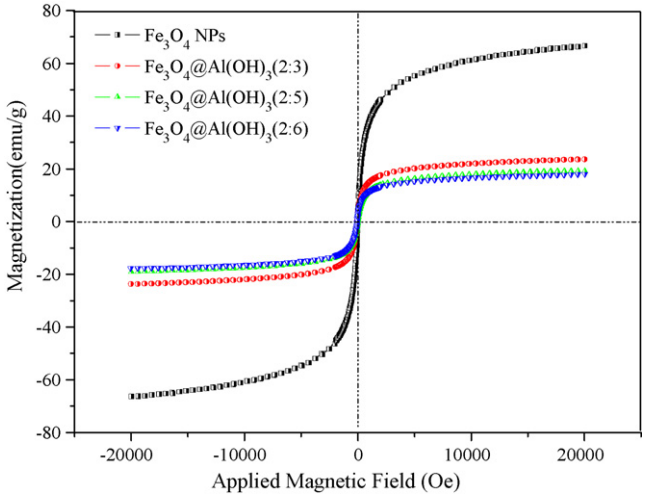

Fig. 5. VSM magnetization curves of Fe_3O_4@$Al(OH)_3$ NPs with various of mass ratio of Fe_3O_4 to $Al(OH)_3$.

The magnetic Fe_3O_4@$Al(OH)_3$ adsorbents possess high affinity toward fluoride. As can been seen from Fig. 6, with the increasing mass ratio of $Al(OH)_3$, the amount of adsorbed fluoride increased remarkably. When the mass ratio of Fe_3O_4 to $Al(OH)_3$ reached 2:5, the adsorption amount of fluoride did not change significantly. $Al(OH)_3$ layer with enough thickness is rather indispensable for adsorption while increase of the $Al(OH)_3$ layer thickness results in the decrease of the magnetic strength. As a compromise, Fe_3O_4@$Al(OH)_3$ (2:5) NPs were selected for further experiments because of high adsorption capacity and strong magnetic property.

3.3. Adsorption behavior and possible mechanism of fluoride

Several researchers have reported the possible adsorption mechanism of fluoride on floc $Al(OH)_3$ which was either by electrostatic adsorption [8,9] or surface complexation [10,30], or a combination of both. The surface of mineral oxides is negative charged when pH value is above the pH ZPC (zero point charge) and positive charged when pH value is below the ZPC. The ZPC of $Al(OH)_3$ was 9.5 [31]. Generally, the charge density that varies strongly with pH is a main factor determining the fluoride load onto the adsorbents surface, and fluoride adsorption is there-

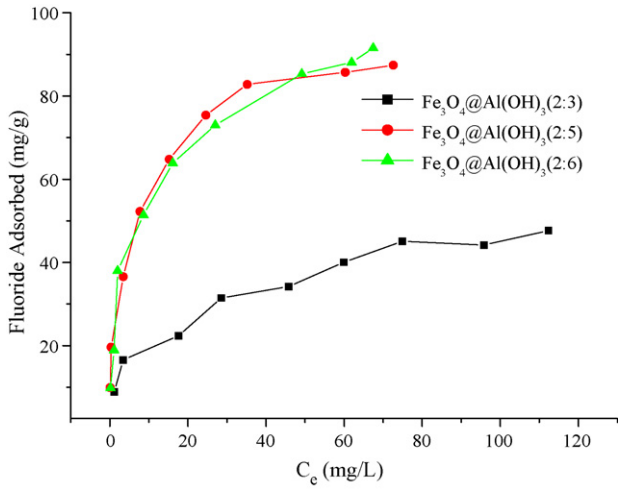

Fig. 6. Equilibrium isotherms of defluoridation by Fe_3O_4@$Al(OH)_3$ NPs with various of mass ratio of Fe_3O_4 to $Al(OH)_3$. Performed in batch mode. pH 6.5, adsorbent: 1 mg mL^{-1}, temperature: 25 °C.

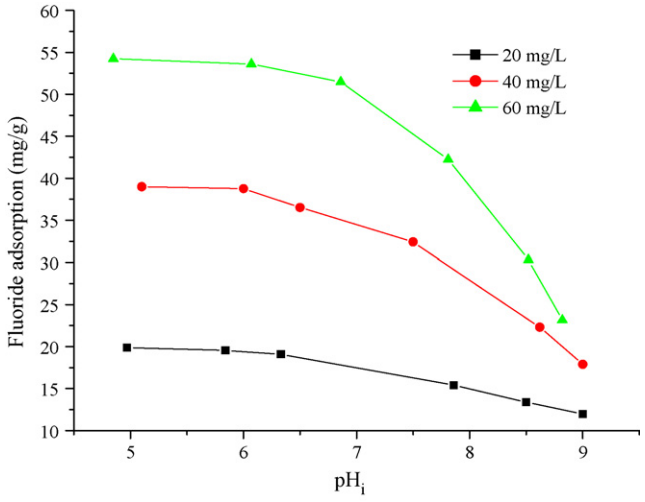

Fig. 7. Effect of initial pH (pH_i) on the adsorption of fluoride by the Fe_3O_4@$Al(OH)_3$ NPs. Performed in batch mode. Adsorbent: 1 mg mL^{-1}, temperature: 25 °C.

fore considered dependent on the initial solution pH. As shown in Fig. 7, the adsorption of fluoride was more favored in acid solution. Fe_3O_4@$Al(OH)_3$ NPs exhibited strong adsorption of fluoride when the pH value was between 5.0 and 7.0, which can be ascribed to the electrostatic attraction between the positive charged Fe_3O_4@$Al(OH)_3$ surface and the anions fluoride. Due to the decrease of charge density, the adsorption efficiency decreased dramatically when the pH was above 7.0. In detail, the surface of magnetic adsorbents became more positively charged while decreasing the pH below its iep. Hence, more fluoride anions were attracted to the surface, causing an increase in the adsorption capacity. Furthermore, during the adsorption progress, the equilibrium pH markedly increased, which might suggest that fluoride has been adsorbed through surface complexation according Eq. (1). Lower initial pH was helpful for their adsorption, which agreed well with the aforementioned possible adsorption mechanism. Since excessively strong acidity was not appropriate for the handling of drinking water samples, neutral solution (about pH 6.5) was selected for further experiments.

XPS spectra of Fe_3O_4@$Al(OH)_3$ (2:5) NPs before and after reaction with fluoride was shown in Fig. 4 (curves b and c). Strong F peaks were observed at 685 and 30 eV, which were respectively assigned to the F 1s and F 2s photoelectrons, indicating that significant F was taken up by the surface. All of the results indicated that the adsorption was driven by both electrostatic attraction and surface complexation.

3.4. Adsorption isotherm analysis

The isotherm models of Langmuir and Freundlich were used to fit the experimental adsorption equilibrium data of fluoride on magnetic adsorbents. These models are represented mathematically as follows [8,9]:

$$\text{Langmuir isotherm}: q_e = \frac{q_m K_L C_e}{1 + K_L C_e} \quad (2)$$

$$\text{Freundlich isotherm}: q_e = K_F C_e{}^{1/n} \quad (3)$$

where C_e (mg L^{-1}) is the concentration of fluoride at equilibrium, K_L (L/mg), and q_m (mg g^{-1}) are the Langmuir constants related to the energy of adsorption and maximum capacity, respectively; K_F (mg$^{1-(1/n)}$ L$^{1/n}$ g^{-1}) and $1/n$ are the Freundlich constants related to the adsorption capacity and intensity, respectively; and q_e (mg g^{-1}) is the mass of fluoride adsorbed per mass of adsorbent. The results of fitting Freundlich and Langmuir equations to isotherm curves are summarized in Table 1. Regression coefficients (r^2) for different conditions were larger than 0.95, indicating that both the models fit reasonably well with the fluoride adsorption. The maximum monolayer adsorption capacity (q_m) obtained for Fe_3O_4@$Al(OH)_3$ (2:5) NPs was 88.49 mg g^{-1} at 25 °C, which was much higher than that of Fe_3O_4@$Al(OH)_3$ (2:3) (q_m = 51.28 mg g^{-1}) but close to that of Fe_3O_4@$Al(OH)_3$ (2:6) (q_m = 91.74 mg g^{-1}). The Freundlich adsorption intensity parameters (n values) were higher than 2, also supporting the favorable adsorption of fluoride on this adsorbents. The surface texture and magnetic properties were not significantly changed when the fluoride were adsorbed on Fe_3O_4@$Al(OH)_3$. The minimum residual concentration of fluoride was 0.3 mg L^{-1} with an initial concentration of 20 mg L^{-1}. Furthermore, after water samples been treated by Fe_3O_4@$Al(OH)_3$ (2:5) NPs, the residual concentration of aluminum was about 0.07 mg L^{-1} at pH 6.5, which met the standard for drinking water quality. Thus, it is suggested that the strong affinity of Fe_3O_4@$Al(OH)_3$ NPs towards fluoride make excellent adsorbents to meet the need of high-fluoride containing aqueous treatment.

3.5. Adsorption kinetic studies

Adsorption kinetics is one of the most important characters which represent the adsorption efficiency. The adsorption rate of fluoride adsorption on the Fe_3O_4@$Al(OH)_3$ (2:5) NPs surface, as a function of the initial fluoride concentration, is shown in Fig. 8(a). Due to faster adsorption kinetics with smaller particles [32], the fluoride adsorption was initially rapid, up to 10 min, after which it decreased. The time required to reach equilibrium was 60 min. The kinetics of fluoride adsorption onto the magnetic adsorbents fit well with the pseudo-second-order kinetic model (r^2 = 0.9990–1.0000).

$$\text{Pseudo-second-order isotherm}: \frac{t}{q_t} = \frac{1}{k_2 q_e{}^2} + \frac{1}{q_e} t \quad (4)$$

where k_2 is the rate constant of adsorption (in g mg^{-1} min^{-1}), q_t is the amount of fluoride adsorbed by adsorbent at any time (mg g^{-1}), q_e is equilibrium adsorption capacity (mg g^{-1}). And the initial sorption rate, h_0 (mg g^{-1} min^{-1}) can be defined as:

$$h_0 = k_2 q_e^2 \quad (t \to 0) \quad (5)$$

Both k_2 and h_0 could be determined experimentally by plotting of t/q_t against t.

Table 1
Langmuir, Freundlich isotherms for fluoride adsorption onto the Fe_3O_4@$Al(OH)_3$ nanoparticles[a].

Parameter	Langmuir isotherm model			Freundlich isotherm model		
Fe_3O_4@$Al(OH)_3$	q_m (mg g^{-1})	K_L (L/mg)	r^2	K_F (mg$^{1-(1/n)}$L$^{1/n}$ g^{-1})	n	r^2
2:3	51.28	0.071	0.974	9.241	2.85	0.978
2:5	88.49	0.294	0.992	25.01	3.12	0.980
2:6	91.74	0.200	0.974	23.9	2.80	0.953

[a] F^- at pH 6.5, adsorbent, 1 g L^{-1}, 25 °C.

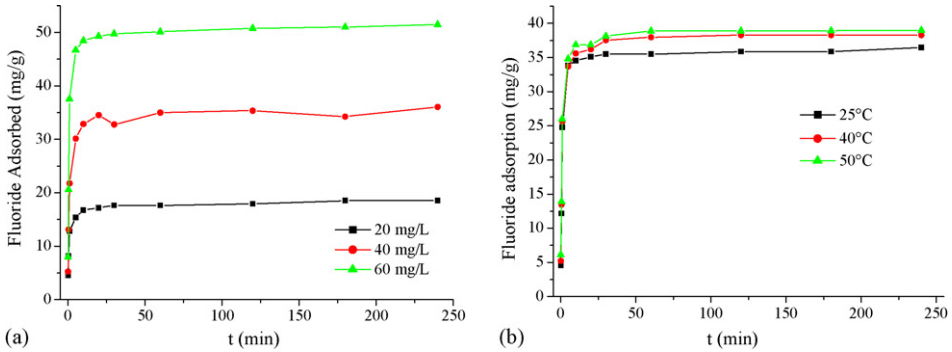

Fig. 8. Effect of contact time on fluoride adsorption rate for different initial F^- concentration (a) and for different temperature (b). Performed in batch mode. pH 6.5, adsorbent: 1 mg mL^{-1}, temperature: 25 °C (a). Initial fluoride concentration: 40 mg L^{-1} (b).

Table 2
Kinetic parameter of pseudo-second-order for fluoride adsorption onto the Fe_3O_4@Al(OH)$_3$ (2:5) nanoparticles.

Parameter	Different initial F^- concentration[a]			Different temperature[b]		
	at 20 mg L^{-1}	at 40 mg L^{-1}	at 60 mg L^{-1}	at 25 °C	at 40 °C	at 50 °C
k_2 (g mg^{-1} min^{-1})	3.142×10^{-2}	2.224×10^{-2}	2.150×10^{-2}	2.601×10^{-2}	3.862×10^{-2}	4.122×10^{-2}
q_e (mg g^{-1})	18.58	35.59	51.55	36.10	38.46	39.06
h_0 (mg g^{-1} min^{-1})	10.86	28.17	57.14	33.90	57.14	62.89
r^2	0.9997	0.9990	0.9999	0.9992	1.00	0.9997

[a] pH 6.5, adsorbent: 1 mg mL^{-1}, temperature: 25 °C.
[b] pH 6.5, adsorbent: 1 mg mL^{-1}, initial fluoride concentration: 40 mg L^{-1}.

Table 3
Thermodynamic parameter for adsorption of fluoride onto the Fe_3O_4@Al(OH)$_3$ nanoparticles[a].

Adsorbent				$-\Delta G^0$ (kJ mol^{-1})			
Fe_3O_4@Al(OH)$_3$	ΔH^0 (kJ mol^{-1})	ΔS^0 (J mol^{-1} K^{-1})	r^2	at 25 °C	at 40 °C	at 50 °C	at 60 °C
2:3	6.310	23.21	0.995	0.605	0.954	1.186	1.142
2:5	6.836	41.65	0.967	5.574	6.199	6.615	7.032
2:6	7.750	48.24	0.979	6.625	7.349	7.831	8.313

[a] Fluoride at pH 6.5, adsorbent, 1 g L^{-1}, initial fluoride concentration: 40 mg L^{-1}.

The initial rapid adsorption was presumably due to electrostatic attraction. The slow adsorption in the later stage represented a gradual uptake of fluoride at the inner surface by complexation or ion-exchange. The constant k_2, the initial sorption rate h_0 and equilibrium adsorption capacity (q_e) obtained from the slope and intercept of plots were presented in Table 2. The results showed decrease in k_2 values and increase in h_0 and q_e values with higher initial fluoride concentrations. The equilibrium adsorption capacity (q_e) evaluated from the pseudo-second-order plot was found to increase from 19.58 to 54.55 mg g^{-1} as the fluoride concentration increased from 20.0 to 60.0 mg L^{-1}, which suggested that the studied magnetic adsorbent would be a good adsorbent for scavenging fluoride from the contaminated water.

The time-dependent adsorption kinetics studies of Fe_3O_4@Al(OH)$_3$ (2:5) NPs were conducted at three different temperatures and analyzed using pseudo-second-order kinetic equations (Eq. (4)). As shown in Fig. 8(b) and Table 2, the constant k_2, the initial sorption rate h_0 and equilibrium adsorption capacity (q_e) values all increased with the increase of temperature from 25 to 50 °C. The increase in adsorption capacity and rate of fluoride with increasing temperature is presumably because of the endothermic nature of fluoride adsorption on magnetic adsorbents [9].

The increase in the pseudo-second-order rate constant with increasing temperature can be described by the Arrhenius equation:

$$\ln k_2 = \ln A + \left(\frac{-E_a}{R}\right)\frac{1}{T} \quad (6)$$

where k_2 is the pseudo-second-order rate constant, A is a temperature-independent factor and E_a is the activation energy of adsorption. The A and E_a obtained from the plot of lnk_2 against $1/T$ were 0.2101 g mg^{-1} s^{-1} and 1.525 kJ mol^{-1}.

3.6. Thermodynamic parameters

The thermodynamic parameters for the adsorption process were calculated using the following relations:

$$\log\left(\frac{q_e}{C_e}\right) = \frac{\Delta S^0}{2.303R} - \left(\frac{\Delta H^0}{2.303R}\right)\frac{1}{T} \quad (7)$$

$$\Delta G^0 = \Delta H^0 - T\Delta S^0 \quad (8)$$

where q_e/C_e is the adsorption affinity; ΔG^0, ΔH^0 and ΔS^0 are the change in free energy, enthalpy, and entropy, under standard states, respectively. The thermodynamic parameters were computed from the plot of log(q_e/C_e) versus $1/T$ for an initial fluoride concentration of 40 mg L^{-1}. The calculated value of ΔH^0 for Fe_3O_4@Al(OH)$_3$ (2:5) NPs was 6.836 kJ/mol, which definitely verify the endothermic nature of the fluoride adsorption process. The ΔS^0 obtained was 41.65 J mol^{-1} K^{-1}. Using the values of ΔH^0 and ΔS^0, the ΔG^0 values have been calculated by Eq. (8) and shown in Table 3, which indicated the adsorption of fluoride was spontaneous and the spontaneity of the process was enhanced with increasing temperature.

Table 4
Langmuir, Freundlich isotherms for fluoride adsorption onto the Fe_3O_4@$Al(OH)_3$ (2:5) nanoparticles in the presence of anions and several real water samples[a].

Parameter	Langmuir isotherm model			Freundlich isotherm model		
Anions or water sample	q_m (mg g^{-1})	K_L (L/mg)	r^2	K_F (mg$^{1-(1/n)}$L$^{1/n}$ g^{-1})	n	r^2
No	88.49	0.294	0.992	25.01	3.12	0.980
NO_3^-[b]	77.99	0.174	0.964	21.52	3.66	0.991
Cl^-[b]	78.12	0.166	0.964	22.64	3.64	0.984
Br^-[b]	76.53	0.198	0.977	023.75	3.96	0.993
SO_4^{2-}[b]	73.49	0.174	0.964	11.389	2.43	0.951
PO_4^{3-}[b]	69.19	0.035	0.853	7.226	2.18	0.971
Tap water	70.42	0.203	0.989	18.91	3.24	0.972
Ground water	68.49	0.240	0.995	20.17	3.19	0.980
Jingmi Canal river	68.03	0.282	0.988	18.58	3.14	0.937

[a] pH 6.5, amount of adsorbent: 1 g L^{-1}, 25 °C;
[b] Concentration of each anions: 50 mg L^{-1}.

3.7. Effect of competing anions

Drinking water contains many ions such as sulfate, phosphate, chloride, bromide and nitrate [6]. They will consequently compete with fluoride anions for the adsorption sites on the magnetic adsorbents surface. The effect of anion on the adsorption of fluoride was studied in batch mode with the concentration of each anion at 50 mg L^{-1}. The results found that the adsorption capacity of Fe_3O_4@$Al(OH)_3$ (2:5) NPs decreased slightly when competing anions were present. Generally, multivalent anions are adsorbed more readily than monovalent anions [7]. As can be seen from Table 4, fluoride removal in presence of anion increased in the order $PO_4^{3-} < SO_4^{2-} < Br^- \approx NO_3^- \approx Cl^-$. It closely correlated with the Z/r (charge/radius) values of the anions which varies in the order PO_4^{3-} (3/3.40) > SO_4^{2-} (2/2.40) > Cl^- (1/1.81) > Br^- (1/1.95) > NO_3^- (1/2.81). All of the results indicated that the Fe_3O_4@$Al(OH)_3$ NPs possessed specific affinity toward fluoride, making it a highly-suitable adsorbent for fluoride contaminated water treatment.

3.8. Adsorption of fluoride from water samples

The potential application of Fe_3O_4@$Al(OH)_3$ NPs for removing fluoride from drinking water was tested by determining the adsorption equilibrium isotherm using ground water and surface water samples. The chemical compositions of water samples were determined and summarized in Table 5. Table 4 lists the maximum adsorption capacity (q_m) obtained for Fe_3O_4@$Al(OH)_3$ (2:5) NPs in the real water samples. Due to competing adsorption of co-existing anions, decreased adsorption capacity of fluoride (Langmuir adsorption capacity was 68 mg g^{-1} for Jingmi Canal river) were observed for all three water samples. Nonetheless, the capacity was still comparable with those obtained by other fluoride adsorbents such as zirconium(IV)-impregnated collagen fiber [2], iron(III)–aluminum(III) mixed oxide [9] and calcined Mg–Al–CO_3 layered double hydroxides [7]. The real water samples spiked with 20 mg L^{-1} fluoride were treated by Fe_3O_4@$Al(OH)_3$ (2:5) NPs, which decreased the residual concentration of fluoride to about 0.7 mg L^{-1}. Taking into account the high adsorption capacity and the low residual amount of fluoride, Fe_3O_4@$Al(OH)_3$ (2:5) NPs was judged to be a suitable adsorbents to treat high-fluoride contaminated water to attain drinking standard quality.

Table 5
Chemical composition and characteristics of the real water samples.

	Tap water	Ground water	Jingmi Canal
Sodium	9.41 mg L^{-1}	23.4 mg L^{-1}	17.1 mg L^{-1}
Magnesium	16.2 mg L^{-1}	1.84 mg L^{-1}	1.66 mg L^{-1}
Calcium	29.4 mg L^{-1}	31.6 mg L^{-1}	25.6 mg L^{-1}
Potassium	1.91 mg L^{-1}	16.5 mg L^{-1}	8.87 mg L^{-1}
Lithium	2.73 μg L^{-1}	6.32 μg L^{-1}	2.94 μg L^{-1}
Barium	74.1 μg L^{-1}	71.5 μg L^{-1}	100 μg L^{-1}
Silica, total	5 mg L^{-1}	8 mg L^{-1}	20 mg L^{-1}
Sulfate	25.5 mg L^{-1}	48.4 mg L^{-1}	25.4 mg L^{-1}
Chloride	20.7 mg L^{-1}	15.3 mg L^{-1}	9.0 mg L^{-1}
Fluoride	0.287 mg L^{-1}	0.829 mg L^{-1}	0.972 mg L^{-1}
Nitrate	8.94 mg L^{-1}	6.87 mg L^{-1}	7.43 mg L^{-1}
Phosphate	<1 μg L^{-1}	<1 μg L^{-1}	2 μg L^{-1}
pH	7.72	7.79	7.97
TOC	0.71 mg L^{-1}	0.58 mg L^{-1}	0.97 mg L^{-1}

4. Conclusions

Compared to previous defluoridation methods, the attractive merits of our method were three-fold: (a) high adsorption capacity and high selective affinity toward fluoride. Sorbents have higher surface areas and shorter diffusion route and the $Al(OH)_3$ surface layer of Fe_3O_4@$Al(OH)_3$ NPs possesses specific affinity toward fluoride, therefore, satisfactory results can be achieved by using less amount sorbents than traditional micron-size particle sorbents. (b) Rapid defluoridation treatment. The superparamagnetic and strong magnetization properties of the Fe_3O_4@$Al(OH)_3$ NPs are favorable for MCT. The treatment process avoids the time-consuming adsorbent bed passing and exhibits great potential in treatment large volume real water samples. (c) Easy preparation, which can meet the need of practical application for treatment of large volume high-fluoride contaminated water.

Acknowledgments

This work was jointly supported by the National Natural Science Foundation of China (20621703), the State High Technology Development Plan (2007AA06A407) and the National Basic Research Program (973) of China (2008CB418200).

References

[1] B.D. Turner, P. Binning, S.L.S. Stipp, Fluoride removal by calcite: evidence for fluorite precipitation and surface adsorption, Environ. Sci. Technol. 39 (2005) 9561–9568.
[2] X.P. Liao, B. Shi, Adsorption of fluoride on zirconium (IV)-impregnated collagen fiber, Environ. Sci. Technol. 39 (2005) 4628–4632.
[3] World Health Organization, Guidelines for Drinking-Water Quality: Incorporating First Addendum Recommendations, vol. 1, 3rd ed., World Health Organization, 20 Avenue Appia, 1211 Geneva 27, Switzerland, 2006, pp. 375–376.
[4] D. Ortiz-Péreza, M. Rodríguez-Martínezb, F. Martínezb, V.H. Borja-Aburtoc, J. Castelod, J.I. Grimaldoe, E. de la Cruze, L. Carrizales, F. Díaz-Barriga, Fluoride-induced disruption of reproductive hormones in men, Environ. Res. 93 (2003) 20–30.
[5] N.A. Medellin-Castillo, R. Leyva-Ramos, R. Ocampo-Perez, R.F. Garcia de la Cruz, A. Aragon-Piña, J.M. Martinez-Rosales, R.M. Guerrero-Coronado, L. Fuentes-Rubio, Adsorption of fluoride from water solution on bone char, Ind. Eng. Chem. Res. 46 (2007) 9205–9212.
[6] E.J. Reardon, Y.X. Wang, A limestone reactor for fluoride removal from wastewaters, Environ. Sci. Technol. 34 (2000) 3247–3253.
[7] L. Lv, J. He, M. Wei, D.G. Evans, X. Duan, Factors influencing the removal of fluoride from aqueous solution by calcined Mg–Al–CO_3 layered double hydroxides, J. Hazard. Mater. B 133 (2006) 119–128.

[8] L. Lv, Defluoridation of drinking water by calcined MgAl-CO_3 layered double hydroxides, Desalination 208 (2007) 125–133.
[9] K. Biswas, S.K. Saha, U.C. Ghosh, Adsorption of fluoride from aqueous solution by a synthetic iron(III)–aluminum(III) mixed oxide, Ind. Eng. Chem. Res. 46 (2007) 5346–5356.
[10] P. Pommerenk, G.C. Schafran, Adsorption of inorganic and organic ligands onto hydrous aluminum oxide: evaluation of surface charge and the impacts on particle and NOM removal during water treatment, Environ. Sci. Technol. 39 (2005) 6429–6434.
[11] C. Castel, M. Schweizer, M.O. Simonnot, M. Sardin, Selective removal of fluoride ions by a two-way ion-exchange cyclic process, Chem. Eng. Sci. 55 (2000) 3341–3352.
[12] Z. Amor, B. Bernard, N. Mameri, M. Taky, S. Nicolas, A. Elmidaoui, Fluoride removal corn brackish water by electrodialysis, Desalination 133 (2001) 215–223.
[13] F. Shen, X. Chen, P. Gao, G. Chen, Electrochemical removal of fluoride ions from industrial wastewater, Chem. Eng. Sci. 58 (2003) 987–993.
[14] N. Hamdi, E. Srasra, Removal of fluoride from acidic wastewater by clay mineral: effect of solid-liquid ratios, Desalination 206 (2007) 238–244.
[15] Y. Wang, E.J. Reardon, Activation and regeneration of a soil sorbent for defluoridation of drinking water, Appl. Geochem. 16 (2001) 531–539.
[16] E. Oguz, Equilibrium isotherms and kinetic studies for the sorption of fluoride on light weight concrete materials, Colloids Surf. A: Physicochem. Eng. Aspects 295 (2007) 258–263.
[17] X.M. Wu, Y. Zhang, X.M. Dou, M. Yang, Fluoride removal performance of a novel Fe–Al–Ce trimetal oxide adsorbent, Chemosphere 69 (2007) 1758–1764.
[18] Y.M. Zhou, C.X. Yu, Y. Shan, Adsorption of fluoride from aqueous solution on La^{3+}-impregnated cross-linked gelatin, Sep. Purif. Technol. 36 (2004) 89–94.
[19] X.L. Zhao, Y.L. Shi, Y.Q. Cai, S.F. Mou, Cetyltrimethylammonium bromide-coated magnetic nanoparticles for the pre-concentration of phenolic compounds from environmental water samples, Environ. Sci. Technol. 1139 (2008) 178–184.
[20] X.L. Zhao, Y.L. Shi, T. Wang, Y.Q. Cai, G.B. Jiang, Preparation of silica-magnetite nanoparticle mixed hemimicelle sorbents for extraction of several typical phenolic compounds from environmental water samples, J. Chromatogr. A 1188 (2008) 140–147.
[21] J.D. Li, X.L. Zhao, Y.L. Shi, Y.Q. Cai, S.F. Mou, G.B. Jiang, Mixed hemimicelles solid-phase extraction based on cetyltrimethylammonium bromide-coated nanomagnets Fe_3O_4 for the determination of chlorophenols in environmental water samples coupled with liquid chromatography/spectrophotometry detection, J. Chromatogr. A 1180 (2007) 24–31.
[22] W. Yantasee, C.L. Warner, T. Sangvanich, R.S. Addleman, T.G. Carter, R.J. Wiacek, G.E. Fryxell, C. Timchalk, M.G. Warner, Removal of heavy metals from aqueous systems with thiol functionalized superparamagnetic nanoparticles, Environ. Sci. Technol. 41 (2007) 5114–5119.
[23] L. Cumbal, A. Sengupta, Arsenic removal using polymer-supported hydrated iron (III) oxide nanoparticles: role of donnan membrane effect, Environ. Sci. Technol. 39 (2005) 6508–6515.
[24] F. Shen, X.M. Chen, P. Gao, G.H. Chen, Electrochemical removal of fluoride ions from industrial wastewater, Chem. Eng. Sci. 58 (2003) 987–993.
[25] D. Leun, A.K. Sengupta, Preparation and characterization of magnetically active polymeric particles (MAPPs) for complex environmental separations, Environ. Sci. Technol. 34 (2000) 3276–3282.
[26] P. Wu, J. Zhu, Z. Xu, Template-assisted synthesis of mesoporous magnetic nanocomposite particles, Adv. Funct. Mater. 14 (2004) 345–351.
[27] T. Sen, A. Sebastianelli, L.J. Bruce, Mesoporous silica-magnetite nanocomposite: fabrication and applications in magnetic bioseparations, J. Am. Chem. Soc. 128 (2006) 7130–7131.
[28] H.R. Zhang, M.E. Meyerhoff, Gold-coated magnetic particles for solid-phase immunoassays: enhancing immobilized antibody binding efficiency and analytical performance, Anal. Chem. 78 (2006) 609–616.
[29] Z.Y. Ma, Y.P. Guan, H.Z. Liu, Synthesis and characterization of micron-sized monodisperse superparamagnetic polymer particles with amino groups, J. Polym. Sci. Polym. Chem. 43 (2005) 3433–3439.
[30] N. Parthasarathy, J. Buffle, W. Haerdi, Study of interaction of polymeric aluminium hydroxide with fluoride, Can. J. Chem. 64 (1986) 24–30.
[31] J. Rosenqvist, P. Persson, S. Sjöberg, Protonation and charging of nanosized gibbsite (α-$Al(OH)_3$) particles in aqueous suspension, Langmuir 18 (2002) 4598–4604.
[32] M. Badruzzaman, P. Westerhoff, D.R.U. Knappe, Intraparticle diffusion and adsorption of arsenate onto granular ferric hydroxide (GFH), Water Res. 38 (2004) 4002–4012.